GEOFLUIDS

Geofluids (2016) **16**, 673–687 doi: 10.1111/gfl.12200

Complexity of hydrogeologic regime around an ancient low-angle thrust fault revealed by multidisciplinary field study

E. M. MUNDY[1], K. DASCHER-COUSINEAU[2], T. GLEESON[1,3], C. D. ROWE[2] AND D. M. ALLEN[4]

[1]*Department of Civil Engineering, McGill University, Montreal, QC, Canada;* [2]*Department of Earth and Planetary Sciences, McGill University, Montreal, QC, Canada;* [3]*Department of Civil Engineering and School of Earth and Ocean Sciences, University of Victoria, Victoria, BC, Canada;* [4]*Department of Earth Sciences, Simon Fraser University, Burnaby, BC, Canada*

ABSTRACT

Co-located and integrated observation of the surface and subsurface is necessary to characterize fault zone hydrogeology. The spectacular cliff-face exposure of the Champlain Thrust fault at Lone Rock Point, Vermont, and a nearby well-field site provides the opportunity for co-located structural and hydrogeologic field observations. We mapped the prominent structural features of the Champlain Thrust fault and discrete groundwater seeps in outcrop, and also drilled through the fault near the outcrop and determined aquifer parameters from aquifer pumping tests. In outcrop, the fault core thickness varies on the meter scale, splays out into multiple strands, and is offset by a minor normal fault. Groundwater seeps are prevalent in the heavily fractured footwall, but limited in the fault core and hanging wall, suggesting that at the cliff face the water table is generally near the fault core and groundwater flow in the hanging wall is limited. Enrichment of more soluble minerals in cemented fault rock associated with older strands of the fault system may play an important role in localizing karst features in the hanging wall. At the well-field site, the Champlain Thrust fault is offset significantly by a high-angle normal fault, the water table is near the surface, and aquifer pumping tests reveal a complex hydrogeologic system, with karst and steep fractures as strong hydraulic conduits in the hanging wall and fault core. The most salient features of the fault zone hydrogeology in the surface and subsurface data are different, but can be integrated into a preliminary conceptual model. Together, the surface and subsurface methods underscore and emphasize the complexity and heterogeneity of the hydrogeology of this low-angle sedimentary fault.

Key words: Champlain Thrust, fault zone, hydrogeology, outcrop mapping, pumping tests, thrust fault

Received 5 March 2016; accepted 25 August 2016

Corresponding author: Tom Gleeson, Department of Civil Engineering, University of Victoria, Victoria, BC V8W 2Y2, Canada.
Email: tgleeson@uvic.ca. Tel: +(250)853-3934. Fax: +(250)721-6051.

Geofluids (2016) **16**, 673–687

INTRODUCTION

Fault zones in the upper crust are known to have a dominant impact on numerous hydrologic processes. Fault zones can affect regional groundwater flow (Mayer *et al.* 2007; Bense *et al.* 2008; Burbey 2008; Kim *et al.* 2014), hydrothermal fluid circulation (Berkowitz 2002; Rowland & Sibson 2004; Davatzes & Hickman 2010; Faulkner *et al.* 2010; McNamara *et al.* 2015), carbon sequestration (Shipton *et al.* 2004; Agosta *et al.* 2008; Dockrill & Shipton 2010; Kampman *et al.* 2012; Tueckmantel *et al.* 2012), emplacement of petroleum resources (Aydin 2000; Sorkhabi & Tsuji 2005), and affect the safety of nuclear waste storage (Bredehoeft 1997; Douglas *et al.* 2000; Mal'kovskii & Pek 2001; Ofoegbou *et al.* 2001). Although fault zones have been extensively studied and conceptual models developed for various geologic settings, the permeability architecture and fluid flow paths of fault zones remain hard to constrain and predict *a priori*. This is because the hydraulic properties of fault zones vary greatly depending on the lithology of the host rock, fault displacement, geologic setting, state of stress, and temporal

evolution of the fault (Smith *et al.* 1991; Scholz & Anders 1994; Caine *et al.* 1996; Lopez & Smith 1996; Bense *et al.* 2013). Moreover, fault components are heterogeneous and anisotropic, with varying permeability temporally and spatially (Faulkner *et al.* 2010). Agosta *et al.* (2008) calculated the permeability of damage zone and fault rocks from the measurements of porosity, pore geometry, and connectivity, but these values are highly variable along a single fault or between fault systems, and the results may be highly dependent on the choice of conceptual model applied to different permeability units. The permeability structure around faults has been approximated by measuring the properties of surrounding wall rocks, damage zone rocks, and rocks of the fault core at core sample scale, and approximating the changes with depth caused by compression under confining pressure (Evans *et al.* 1997; Wibberly 2002). These estimates can be compared to larger-scale field measurements where available, but the extrapolation to field scale is compromised by the scale-dependent heterogeneity of natural fault systems.

Faults in carbonate rocks exhibit a broad range of hydrogeologic behaviors from effective conduits due to dissolution weathering, dilatational jogs, and uncemented fracture networks (Andrews *et al.* 1982; Billi *et al.* 2007; Bense *et al.* 2013), to significant barriers due to smearing of low-permeability material (e.g., clay gouge) into the fault core (Agosta & Kirschner 2003; Doan & Cornet 2007). Secondary cementation (Micarelli *et al.* 2006), the formation of fine-grained cataclastic fault rocks (Agosta & Kirschner 2003; Celico *et al.* 2006), as well as combined conduit–barrier systems, have been recorded in carbonate rock faults and siliciclastic sedimentary rocks (Allen & Michel 1999; Bense & Person 2006; Breesch *et al.* 2009). Carbonate rocks are susceptible to both dissolution and cementation, to a greater degree than silicate rocks. Therefore, their permeability structure is particularly difficult to predict.

Research on fault zone hydrogeology is sometimes hindered by a lack of synergy between structural geologists and hydrogeologists. Both aim to characterize the fluid flow around fault zones, yet the two disciplines concentrate on different field areas and use diverse methods that integrate over different scales (Ball *et al.* 2010; Bense *et al.* 2013). Structural geologists often focus on surface studies, investigating outcrops that can scale up to hundreds of meters in scale, or analyzing rock samples. Hydrogeologists usually focus on subsurface data, using pumping tests, geochemical surveys, and geophysical data from wells and springs to determine aquifer parameters on local to regional scale (Ball *et al.* 2010; Bense *et al.* 2013). Well-exposed fault zones in outcrop are generally located in areas where a dense network of wells needed for hydrogeologic investigations is not feasible, as these areas are less developed. However, well networks are seldom where we need them and are predominately placed in well-developed areas, where well-exposed outcrops needed for structural geology measurements are sparse (Ball *et al.* 2010; Bense *et al.* 2013). Some studies integrate surface and subsurface data sets to study fault zone hydrogeology, such as geothermal studies (Revil *et al.* 2015; Chambefort *et al.* 2016; McNamara *et al.* 2016; Mroczek *et al.* 2016).

The remarkable exposure of the Champlain Thrust fault at the edge of Lake Champlain at Lone Rock Point in Burlington, Vermont, allows for both structural and hydrogeologic field observations, providing direct data about the lithology, architecture, and hydrogeology of the fault. The Champlain Thrust fault is a surface expression of the frontal thrust of the Taconic Orogeny, which emplaced the Lower Cambrian Dunham dolostone over the Middle Ordovician Iberville shale (Rowley & Kidd 1981; Stanley 1987; Hayman & Kidd 2002). The hydrogeology of the Champlain Thrust has never been studied before and thus represents a unique opportunity to report on the hydrogeology of thrust faults in carbonate settings where mechanically distinct units are juxtaposed.

The objective of this study was to establish a preliminary understanding of the hydrogeology of a low-angle thrust fault in sedimentary rocks, using a multidisciplinary approach. We describe the prominent structural features of the Champlain Thrust fault at the Lone Rock Point outcrop. Hydrogeologic observations from groundwater seeps exposed along the outcrop are presented and related to the structural features in an attempt to establish a correspondence between fault structure and groundwater flow. Aquifer pumping tests in the hanging wall and fault are interpreted from two wells drilled near the outcrop. Rock core was obtained from one of these wells to complement the outcrop structural analysis.

CHAMPLAIN THRUST FAULT

The Champlain Thrust fault extends from southeastern Quebec to the Catskill Plateau in east-central New York (Rowley 1983; Stanley & Ratcliffe 1983, 1985; Ratcliffe *et al.* 2011). It is the southern extension of the larger Logan Line thrust system marking the frontal thrust of the Taconian Orogeny of Middle to Late Ordovician age (Fig. 1; Rowley & Kidd 1981; Stanley 1987; Hayman & Kidd 2002). North of Burlington, USA, the orientation of the Champlain Thrust fault is relatively consistent, striking north and dipping approximately 15 degrees eastward. South of Burlington, the fault has been deformed by high-angle faults and broad folds, making the trace irregular. The displacement along the Champlain Thrust fault is estimated to be 60–80 km, along an azimuth of approximately 300° (Stanley 1987).

The fault is exposed on the shore of Lake Champlain over a roughly 1-km-long segment at Lone Rock Point,

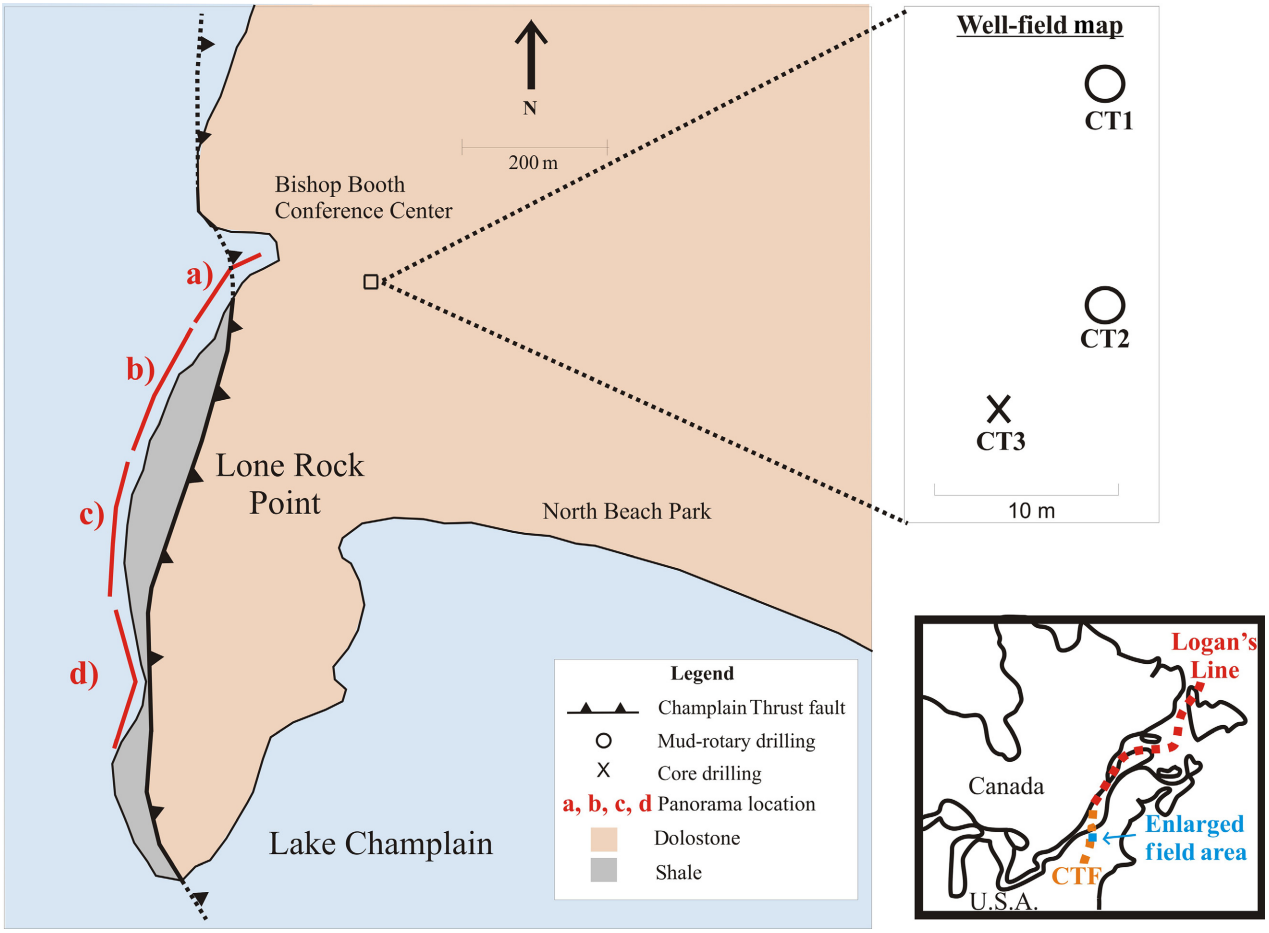

Fig. 1. Location of Champlain Thrust fault and well-field (modified from Stanley 1987) with well locations shown in the upper inset and the location of panoramas (Fig. 2A–D) outlined in red. The regional setting of the Champlain Thrust fault (CFT) and the Logan's Line shown in the lower inset. CT1 and CT3 are pumping wells, whereas CT2 is an observation well.

Burlington, Vermont (Stanley 1987) (Fig. 1). Here, the thrust strikes north–northeast and dips shallowly to moderately to the east. The fault juxtaposes the Lower Cambrian Dunham Formation (hanging wall) over the Middle Ordovician Iberville Formation (footwall). The stratigraphic throw is estimated to be 2700 m (Stanley 1987). Contrasts in erosional competencies cause the hanging wall to be undercut by lake erosion (Stanley 1987).

FAULT GEOMETRY FROM OUTCROP

We mapped the outcrop of the Champlain Thrust at Lone Rock Point on panoramic photographs taken from the frozen lake (Fig. 2), and recorded the lithologic and orientation characteristics of the fault surface along approximately 700 m of strike section. We documented the structural style of the fault, especially focusing on changes in width, orientation, or character of the fault rock along strike. We sampled the fault rock, hanging wall, and footwall rock, to determine the microstructure by optical petrography and mineralogy by bulk powder X-ray diffraction (XRD) performed on the Rigaku SmartLab at McGill University.

The hanging wall is beige crystalline dolostone of the Dunham Formation, crosscut by open fractures, and calcite and dolomite veins. The footwall marl of the Iberville Formation is pervasively folded and crosscut by joints and veins in the vicinity of the Champlain Thrust. Bedding is approximately 1- to 3-cm-thick, alternating massive fine-grained limestone and dark gray to black marly shale, cut by white calcite veins that are most abundant in fold hinge zones. The folds in the footwall shale are typically tight to isoclinal, shallowly plunging with shallowly dipping axial planes. The footwall is cut by brittle faults in diverse orientations, most of which do not cut across the fault into the hanging wall. These structures were described in detail by Stanley & Sarkesian (1972). X-ray diffraction results show that the hanging wall dolostone is 85% dolomite with minor calcite, quartz, and illite, while the footwall contains

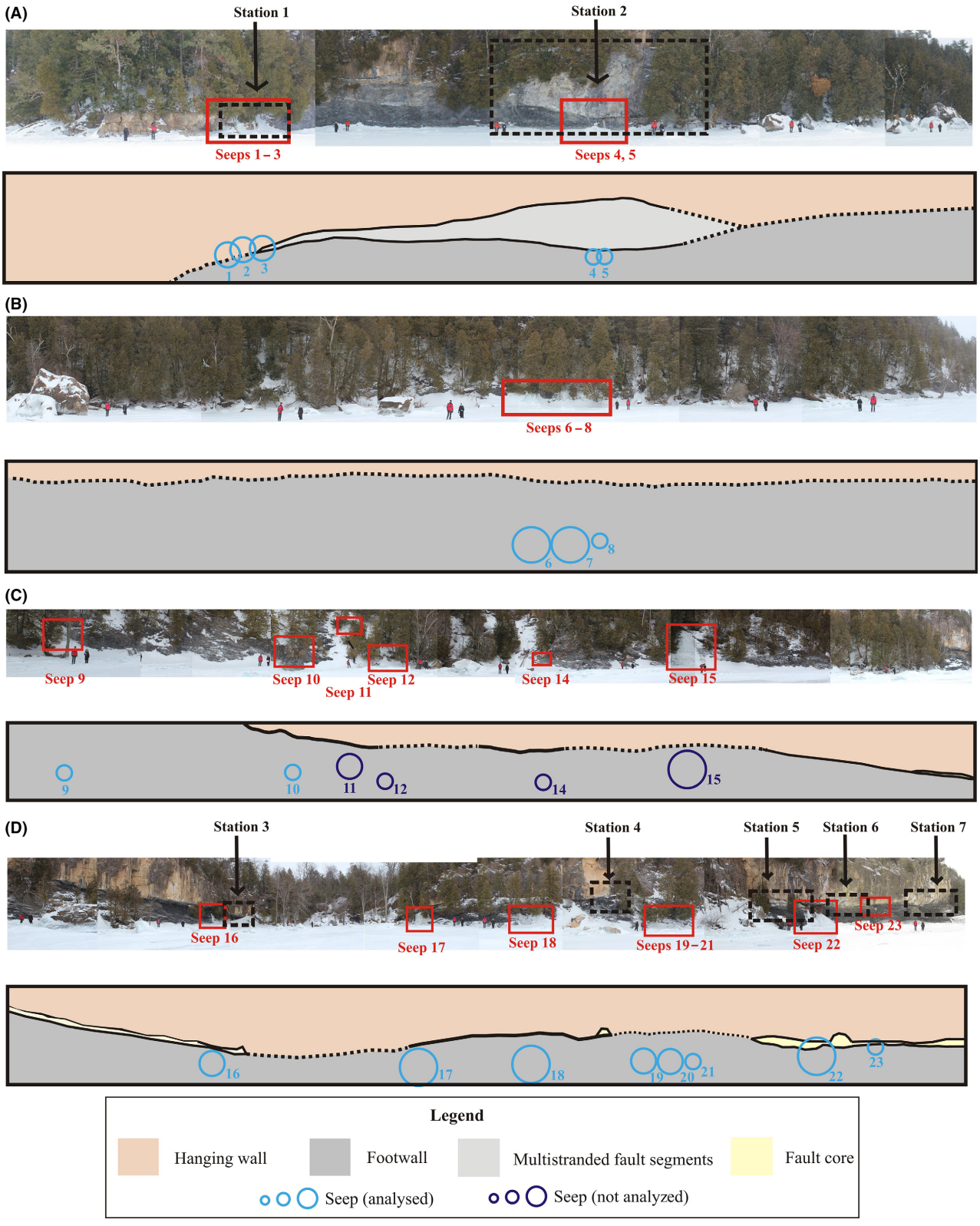

Fig. 2. Panorama of the Champlain Thrust fault. The panorama was shot from the frozen lake surface, from north (A) to south (D). Areas with prominent structural features are outlined in black, and frozen seeps locations are outlined in red (See Fig. 1 for placement on map). Scaled circles represent the small, medium, and large flows observed from the frozen seeps, with the number corresponding to seep number. Scale is defined by people at the base of the fault. Total length of panorama is approximately 700 m.

approximately 75% calcite, 15% quartz, and 10% illite and other phyllosilicates (Table 1, samples D1 and S2, respectively).

The fault core of the Champlain Thrust is a zone of deformed fault rock that contains a mixture of hanging wall and footwall components, calcite and dolomite veins, and brecciated/reworked vein fragments. The color varies from black to gray to beige, is locally massive within lenses of breccia, and is locally foliated with asymmetric S-C fabric. The contact between fault rock and the hanging and footwall is sharp and undulating.

At the outcrop study site, the fault core normally consists of 0.1–0.4 m of fault rock, cut by one sharp continuous fracture surface, interpreted as the principal slip surface (Fig. 3A). The principal slip surface usually divides the hanging wall from the fault core, but locally where the fault core thickens, the principle slip surface crosscuts the fault rock (older breccias and foliated cataclasites) before rejoining the hanging wall interface. The average principal slip surface plane is oriented 017°/11°E, with variations of approximately 16° in strike and approximately 4° in dip corresponding to the meter-scale corrugations on the hanging wall surface ($n = 27$). Based on the crosscutting relationship with other rocks of the fault core, we interpret this discrete surface as likely the latest surface of active slip in the Champlain Thrust.

Several steep normal faults of displacements <10 m, and a few of displacements >10 m, postdate and offset the Champlain Thrust in the study area. These faults contain angular fault breccias partially cemented by porous chalky calcite and are readily distinguishable in outcrop and in drill core from the original Champlain Thrust fault rocks.

At the northern exposure of the Champlain Thrust fault, the main fault core splays out into a network of synthetic anastomosing faults in a zone roughly 3 m thick in the north, increasing to 8 m thick over a approximately 30-m-long segment of the fault (station 2, Figs 2A and 3B), herein referred to as 'multistranded fault segments'. The southern along-strike transition from a discrete fault surface to the south into this complex multistranded segment

Table 1 X-ray diffraction semiquantitative mineralogy.

		Abandoned fault rock in HW (breccia and mylonite)				Along fault core		Abandoned fault rock in FW (mylonite)			
	HW										FW
Mineral	D1	S7	S8	S10	S14	S4	D2	S1	D3	D4	S2
Dolomite	85	0	20	55	5	75	65	35	70	50	0
Quartz	5	Trace	Trace	25	0	Trace	5	20	5	15	15
Illite	5	15	5	Trace	0	5	Trace	5	5	35	10
Calcite	5	85	75	15	95	15	30	40	20	0	75
Expanding clays	0	0	0	Trace	0	Trace	0	0	0	0	
Total (%)	100	100	100	95	100	95	100	100	100	100	100

HW, hanging wall; FW, footwall. Modal estimate error is not quantitatively constrained, so estimated percentages are rounded to the nearest 5%.

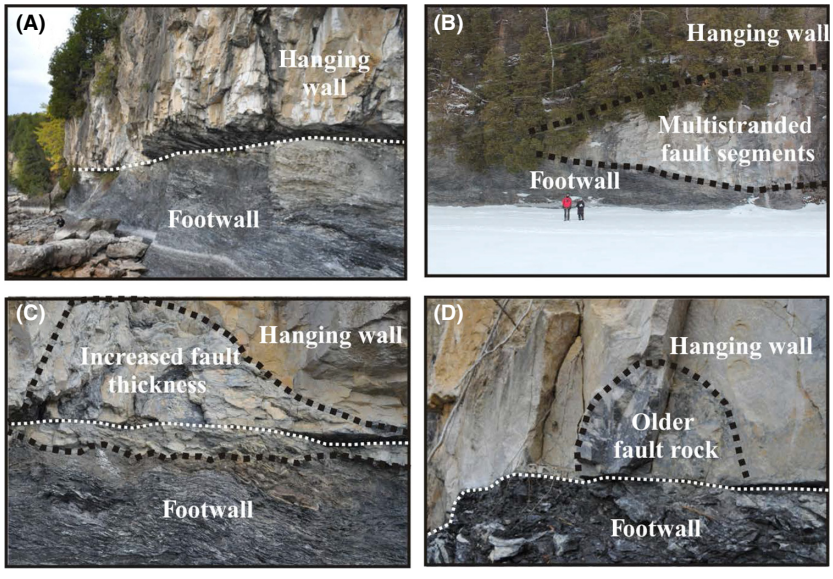

Fig. 3. Main structures observed at Champlain Thrust fault: (A) principal slip surface, (B) multistranded fault segments (station 2 in Fig. 2A), (C) increased fault thickness (station 6 in Fig. 2D), (D) older abandoned fault rock (station 4 in Fig. 2D). Thin dashed white line follows the principal slip surface; thicker black dashed line follows main structural features.

is not exposed. To the north, the Champlain Thrust fault is cut by a normal fault and down-dropped below lake level (station 1, Fig. 2A). The normal fault surface is stepped, striking 306° with dips ranging from 50° to 89°. The fault rock between slip surfaces of the splays is texturally diverse. Large imbricate lens-shaped blocks of fault rock, isolated by bounding synthetic faults, weather dark to pale gray.

Steep-walled embayments filled with older fault rock occur in the hanging wall dolostone directly above the principal slip surface, which truncates them. These are variably sized (20–40 cm wide by 20–40 cm thick) and composed of cohesive cataclasite (station 3–station 6, Figs 2D and 3D). On fresh surfaces, it is possible to distinguish variably sized (<5 cm), randomly oriented clasts in a dark blue crystalline matrix, but on weathered surfaces, the matte beige surface of the healed breccias is almost indistinguishable from the surrounding hanging wall dolostone. These occurrences of relict fault rock preserved in hanging wall embayments were only observed on the sections of the fault where the hanging wall had recently collapsed, exposing large fresh surfaces above the fault. Mineralogy determined by XRD (Table 1, Samples S7, S8, S10, S14) shows that calcite is enriched in these healed breccias, indicating that dolostone fragments were cemented by calcite veins during fault rock healing.

Three areas of the exposure show localized abrupt thickening of the fault core (station 3, station 6, station 7, Figs 2D and 3C), accommodated by concavities in the hanging wall surface. The fault core at station 7 (Fig. 2D) reaches up to 3 m thick. The best exposed example is at station 6 (Fig. 2D). The fault rock thickens to more than 2.5 m over 3 m in strike length. The geometry of the thickened section is asymmetric; the left side dips steeply into the main fracture, while the right side tapers into it. The principal slip surface cuts through the middle of the thickened fault rock. The southernmost recorded occurrence of a thickened section of the fault core is at station 3 (Fig. 2D). Here, the fault rock thickens to approximately 0.5 m over a 2-m segment of the fault. The transition from normal fault core thickness to the thickened section is gradual to both the north and south.

Given the field observations collected at the Champlain Thrust fault, it is evident that the fault core structure thickness and rock type change on the scale of a few meters, over an outcrop study length of approximately 700 m (Fig. 4). The preserved fault zone architecture is the cumulative effect of the entire history of fault motion, as well as the more recent effect of steep normal faults offsetting the original thrust plane. The nearly complete healing of early fault breccias in hanging wall embayments, and elevated concentrations of calcite in the healed breccias, indicates that ancient fluid flow played an important role in re-sealing and healing the fault while it was still active. The fault rock contains variable proportions of dolomite, calcite, quartz, illite, and other phyllosilicates (Table 1, samples S4 and D2). The source of dolomite to the fault rock is comminuted hanging wall dolostone. Calcite, quartz,

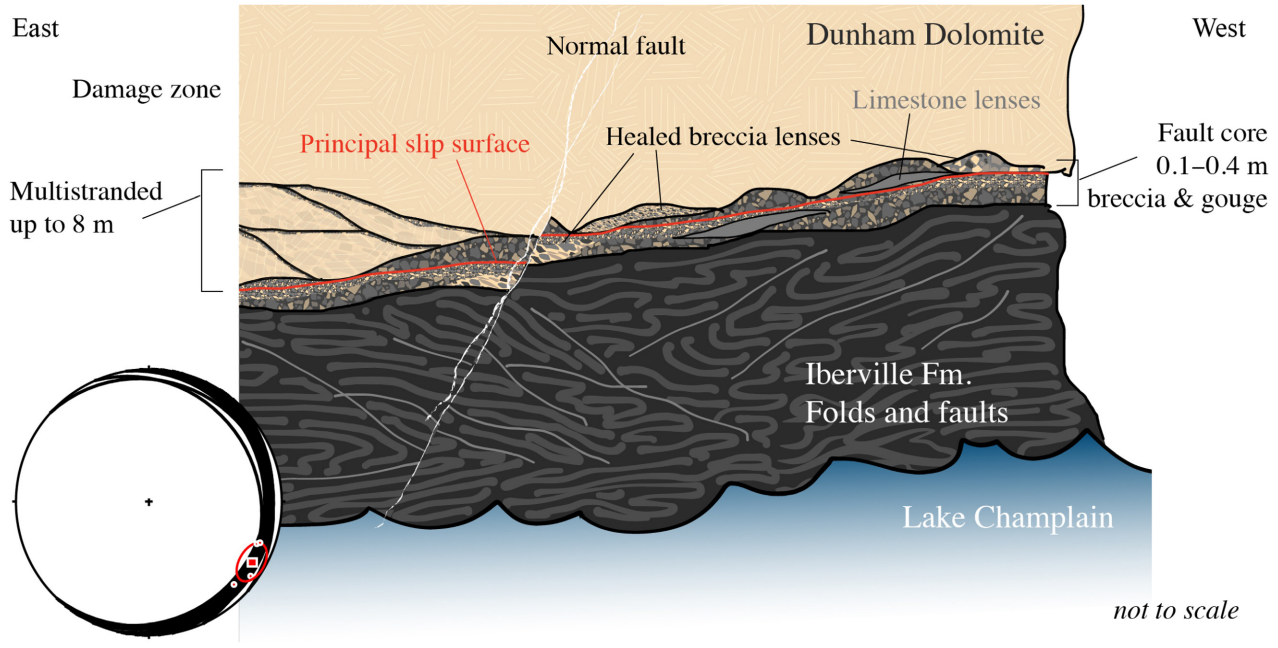

Fig. 4. Schematic model showing structural features of the Champlain Thrust. Stereonet shows measured orientations of the principal slip surface (n = 27) and axes of corrugations on the base of the hanging wall (n = 4), which are a proxy for slip direction.

and illite are sourced from comminution of footwall marls. When calcite proportion within fault rock exceeds the proportions of quartz and illite, this indicates that the calcite was introduced as veins and cements rather than fragments of footwall rock. Excess calcite occurs dominantly in the healed fault rock in the hanging wall (Table 1, samples S7, S8, S14), recording calcite cementation of previously formed breccias.

The crosscutting relationship between the healed breccias and the principle slip surface shows that following healing, the fault slip was more localized onto a discrete slip surface. The variations in fault architecture, such as splaying into multiple strands or broadening of the fault core, may contribute to the present-day permeability structure of this ancient fault. For example, the calcite-cemented volumes of older fault rock are likely significantly more soluble in fresh water than the surrounding dolostone and so may influence the evolution of karst systems as discussed below.

LOCALIZED GROUNDWATER FLUX FROM ICE SEEPS

Groundwater seeps are common along cliff faces of fractured and faulted rock, as fractures provide a pathway for fluid flow out of the subsurface. The distribution and flux of groundwater seepage is a function of the distribution of permeability (Deitchman & Loheide 2009), which in fractured bedrock is controlled by fracture networks. Thus, examining seeps can provide valuable information about the fracture networks and permeability of the rock mass, in addition to providing a minimum elevation of the water table. Detailed observations of frozen seeps in an abandoned quarry in a similar climate indicate that the seeps can freeze over in extreme cold events (<−20°C), but generally the groundwater inexorably flows onto the cliff face, slowly increasing the volume of the frozen seep when air temperatures are below 0°C (Mundy *et al.*, submitted). Therefore, the cumulative volume of the frozen seep after a period of freezing temperatures is a time-integrated average of the groundwater flow from that seep.

In February 2014, the Lone Rock Point thrust fault outcrop was surveyed for frozen groundwater seeps from the frozen surface of Lake Champlain. Detailed surveys were made in the footwall throughout the outcrop, but were not possible at the fault and hanging wall in some areas due to the difficulty of access. Twenty-three ice seeps were identified, of which 19 were readily accessible and therefore selected for groundwater flow analysis (Fig. 2, Table 2). In addition to optical photographs, physical observations, such as seep location, notable geologic features, and seep ice deposit height, width, and depth, were recorded. The seep height, width, and depth were used to approximate the volume of groundwater at each seep (Table 2). These volumes were then used to estimate the flow of each seep, using an estimate of time it took to freeze the seeps, determined from air temperature in the weeks preceding the site visit (approximately 3 weeks). As the hanging wall and fault were inaccessible at the southern section of panorama (a), panorama (b), and northern section of panorama (c) (Fig. 2), the number of seep observations may be biased toward the footwall.

The majority of the ice seeps (approximately 70%) occurred in the footwall, suggesting that the heavily fractured and folded footwall has localized permeability pathways. Three seeps occurred in the hanging wall in the section where a later normal fault has down-dropped the hanging wall near the lake level (station 1, Fig. 2). Two seeps occurred at the location where the fault core expands into multiple splays (station 2, Figs 2 and 5A). Two seeps occurred in the fault core (Fig. 5B). The occurrence of seeps at fault intersections like these indicates that the faults in these areas may be acting as conduits, channeling groundwater flow out of the subsurface. No seeps were found in the older, healed fault breccias, so we infer that these breccias are sufficiently healed that the remaining open fracture density is similar to the surrounding fractured dolostone, and there is no increased likelihood of fluid flow through the healed breccias.

On average, ice seeps in the footwall had the largest groundwater flow, which could be due to higher permeability or a higher water table gradient because the footwall is at lower elevations (Table 2). The seeps in the hanging

Table 2 Location of ice seep, approximate volume, and flow.

Seep number	Seep location	Seep height above Lake Champlain (m)	Approximate volume (m^3)	Flow (m^3 sec^{-1})	Sum of seep flows (m^3 sec^{-1})
1	Hanging wall*	1.8	0.408	2.25E-07	1.75E-5
2	Hanging wall*	1.8	0.202	1.11E-07	
3	Hanging wall*	1.8	0.218	1.20E-07	
4	Fault core	1.0	0.001	7.42E-10	
5	Fault core	1.5	0.013	7.29E-09	
6	Footwall	2.0	14.57	8.03E-06	
7	Footwall	2.0	0.735	4.05E-07	
8	Footwall	2.1	0.006	3.27E-09	
9	Footwall	2.7	0.019	1.07E-08	
10	Footwall	2.4	0.063	3.46E-08	
13	Footwall	1.8	0.153	8.41E-08	
16	Footwall	1.9	0.264	1.46E-07	
17	Footwall	2.3	2.17	1.19E-06	
18	Footwall	2.2	1.79	9.88E-07	
19	Footwall	2.1	0.540	2.98E-07	
20	Footwall	2.1	0.119	6.59E-08	
21	Footwall	2.1	0.052	2.88E-08	
22	Fault core	2.7	10.45	5.76E-06	
23	Fault core	3.4	0.007	3.87E-09	

*Down-section of normal fault.

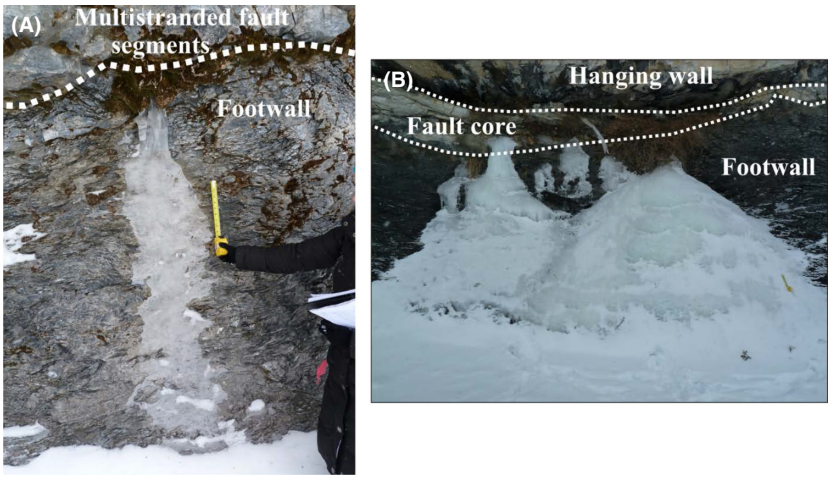

Fig. 5. Optical photograph of (A) seep 5 (located at the intersection between the multistranded fault segment structure and the footwall) and (B) seep 22 (originating in the fault core). Thin dashed white line follows the principal slip surface. Note measuring tape for scale (1 foot). See Fig. 2 for locations.

wall had the second largest flow, followed by the seeps in the fault core. The fault core itself had one large seep that had a large flow (5.76×10^{-6} m sec^{-1}), but on average, the flows from the fault core were less (in the range of 10^{-9} and 10^{-10} m sec^{-1}). There is no discernable relationship between seep flow and elevation, suggesting that water table gradient is not the primary control on seep flow.

Groundwater seeps provide a minimum elevation of the water table. The only seeps in the hanging wall (seeps 1–3) were found where the hanging wall is near the lake elevation due to a late normal fault. The lack of seeps in the hanging wall suggests that the water table at the outcrop is approximately at the elevation of the fault or below.

FAULT GEOMETRY AND HYDROGEOLOGY FROM WELL DATA

Drilling and aquifer pumping tests can reveal fault geometry as well as quantify fracture density, hydraulic connections, and the hydraulic parameters of an aquifer. Rock core retrieved from boreholes can also be used for determining rock stratigraphy and fracture density.

Two wells, CT1 and CT2 (diameter: 0.15 m), were drilled vertically along strike in November 2013 (Fig. 1). Rock chips were collected from the wells at discrete depths at 1.5-m intervals to determine the rock lithology with depth. Both wells were drilled through the fault (Fig. 6A). In CT1, rock chips of hanging wall dolostone were recovered from 6.4 to 25.9 m, with the fault at approximately 27.4 m. A void of 1.83 m was present below the fault (probably due to karst), which terminated drilling below this depth due to pressure losses. In CT2, the hanging wall was recorded from 8.2 to 69.8 m below surface, with the fault at approximately 69.9 m. At approximately 70 m, the footwall is present and continues to the end of the well (152.4 m). The large difference in fault depth between the two wells (>40 m) may be due to the normal fault (striking 306° with dips ranging from 50° to 89°) present at station 1 in Fig. 2. Although the projection of the fault from the beach exposure toward the well-field site is uncertain, it is possible that the fault or a related, similarly oriented fault passes directly between these two well locations.

In March 2014, a third well was drilled using diamond drilling, yielding rock core for lithological and structural analyses. Similar to CT1, a void was present in CT3 (2.13 m) at approximately 38.1 m, resulting in the termination of drilling. Due to this, CT3 did not reach the fault core of the Champlain Thrust fault. The hanging wall rock was composed of fresh gray to buff-colored dolostone with light gray to white crystalline carbonate veins. At 36.6 m, the core degraded into chalky, friable, and weathered rock, possibly similar to the weathered breccias observed in the fault outcrop. This, and the increased frequency of fractures at this depth (measured from rock core, Fig. 7), consistent with the characteristic pattern of a fault damage zone (Savage & Brodsky 2010), suggests that the drilling ended at or very near the main fault and that the rocks were subject to local dissolution by groundwater.

The wells were completed using 0.61-m polyvinyl chloride (PVC) piezometers in October 2014 (Fig. 6B). CT1 was screened at the fault (24.4–27.4 m) and sealed with sand and bentonite. CT2 was completed with two piezometers; one was screened at the fault (67.1–73.2 m), and the other was screened in the footwall (91.4–121.9 m). A layer of sand was placed around each screen and then sealed with a layer of bentonite. CT3 was screened in the hanging wall (32–38.1 m) and completed with a layer of sand and bentonite around and above the screen, respectively.

We observed strong hydraulic connections during drilling and the installation of piezometers in the wells. During the drilling of CT2, at approximately 38.1 m, bubbles

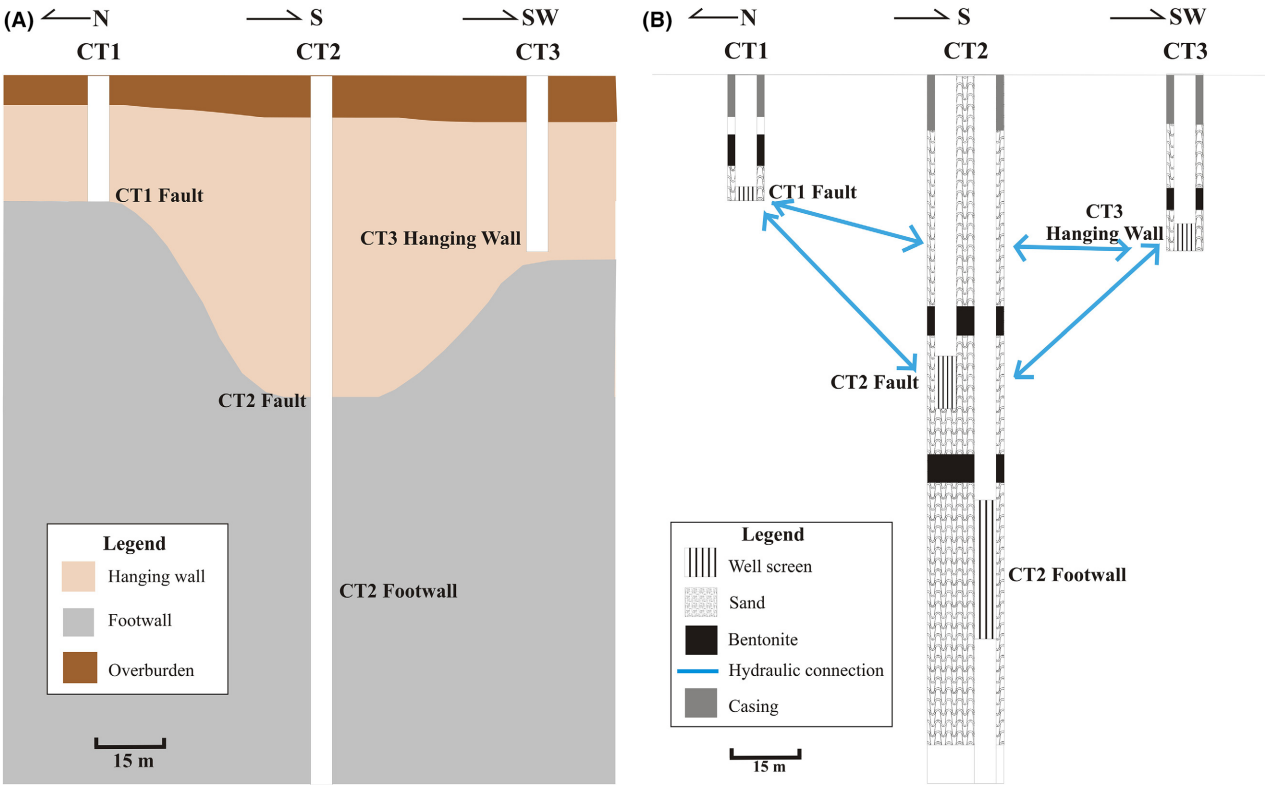

Fig. 6. Cross-section of (A) geology, (B) well completion and hydraulic connection observed from well drilling and piezometer installation.

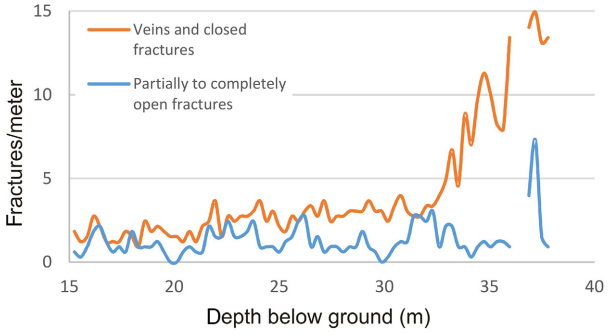

Fig. 7. The number of fractures per foot (0.3) below surface in the hanging wall of the Champlain Thrust. Fractures are classified as veins/closed fractures (certainly ancient) and partially to completely open (may be artificially enhanced by drilling damage). The pattern of increasing fracture abundance toward the bottom of the core is clear in both data sets, similar to well-documented fracture density that increases near fault surfaces (Savage & Brodsky 2010).

appeared in the groundwater-filled trench (made by drillers for mud circulation) beside CT1, and the ground surrounding CT1 began to heave and collapse. Additionally, while installing the piezometer in CT3 (at 36.6 m), water overflowed from the piezometers in CT2 (fault) and CT1 (fault). This suggests that as the piezometer advanced to greater depth, groundwater was being displaced through a conduit that connects the wells, leading to flowing artesian conditions in CT2 (fault) and CT1 (fault). These observations, together with the void space noted during drilling (resulting in pressure losses), suggest that there may be a karst network connecting these depths, creating the pathways for groundwater to flow out of the nearby piezometers. Karst was not reported in previous studies of the Champlain Thrust fault in Burlington (Rowley 1983; Stanley & Ratcliffe 1983, 1985; Stanley 1987) and was not noted in our surface outcrop studies. However, microkarst is present in the Dunham Formation in the Briton Quadrangle in Connecticut, which is caused by solution enlargement of fractures in fracture zones (J. Kim, personal communication). The role of karst in groundwater flow at the Champlain Thrust fault is difficult to constrain, because the distribution of subsurface karst conduits cannot be mapped from the surface or predicted from structural observations.

Aquifer pumping tests were completed in CT1 (fault) and CT3 (hanging wall) in May 2015 using a Grundfos Redi-Flo 2 pump. The aquifer pumping test in CT1 (fault) was completed for 12 h at a pumping rate of 270 ml sec^{-1}, while the aquifer pumping test in CT3 (hanging wall) was completed for 9 h at a rate of 330 ml sec^{-1}. The tests in CT2 fault and footwall were unable to be completed due to pump limitations (the

pump could not lift water from the needed depths at low enough flow rates to sustain a pumping test). Solinst-level loggers were placed in the nonpumping (observation) wells to record the water-level changes throughout the aquifer pumping test and manual water-level measurements were made in the pumping well during the test. The hydraulic properties of the aquifer were determined using Aqtesolv, an aquifer-testing analysis software (Duffield 2007). Various analytical models were explored because no single model could best explain the pumping test responses in these wells given their varied placement with respect to the Champlain Thrust fault, the structure offsetting the Champlain Thrust fault, and the potential karst. This suggests that the hydrogeology of the area is complex and that an integrated conceptual model, combining surface and subsurface observations, is needed. Accordingly, the most appropriate analytical model for each test was used to solve for the aquifer parameters (Tables 3 and 4). We acknowledge that using a variety of analytical models is not ideal; however, analyzing the system using different analytical models allows for the different response types to be identified and related to the geological structure of the area.

The best model to explain the response from the CT1 (fault) aquifer pumping test is the vertical fracture model from Gringarten & Witherspoon (1972) (Table 3; Figure S1). The derivative (Spane and Wurstner, 1993) and the drawdown curve of the pumping well CT1 fault are linear throughout most of the tests, suggesting that a dominant fracture (likely vertical, but possibly horizontal) intersects the pumping well or is situated close by. The pumping test responses at the three observation wells (CT2 fault, CT2 hanging well, and CT3 hanging wall) are all appropriately modeled using the Gringarten–Witherspoon method for observation wells that are situated at some distance to the vertical fracture. The hydraulic conductivity calculated from CT3 (where $K = T/b$, using an aquifer thickness of $b = 6.096$ m) is characteristic of limestone/dolostone (10^{-6} to 10^{-9} m sec^{-1}; values obtained in Freeze & Cherry 1979), while the hydraulic conductivity calculated from CT2 (footwall) is higher than expected for intact shale formations, which is 10^{-9} to 10^{-13} m sec^{-1}. However, the footwall (as observed from the outcrop) is heavily fractured and faulted. Unsealed fractures and faults would provide extra pathways for fluid flow, increasing the hydraulic conductivity of the formation. This is most likely the case for CT2 (footwall). The hydraulic conductivity values calculated from CT1 (fault) and CT2 (fault) are very similar. The average specific storage value (1.95×10^{-4} m^{-1}) of the aquifer as determined from the results for CT3 (hanging wall), CT2 (fault), and CT2 (footwall) is characteristic of confined aquifers, with higher values obtained for the CT2 (fault and footwall) compared to CT3 (hanging wall). The specific storage of the aquifer as determined from the CT1 (fault) is not representative of the aquifer because the method simply uses the radius of the pumping well.

Table 3 Hydraulic conductivity and specific storage of each well during the 12-h CT1 fault pumping test.

Hydraulic Property	CT1 fault (pumping well)	CT2 fault	CT2 footwall	CT3 hanging wall
K (m sec^{-1})	1.43E-06	2.05E-06	2.05E-06	4.52E-06
S_s (m^{-1})	–	2.98E-04	2.84E-04	1.94E-06

Table 4 Hydraulic conductivity and specific storage of each well during the 9-h CT3 hanging wall aquifer pumping test.

Hydraulic Property	CT3 hanging wall (pumping well)	CT1 fault	CT2 fault	CT2 footwall
K (m sec^{-1})	1.22E-06	4.56E-07	5.65E-08	1.34E-06*
S_s (m^{-1})	–	1.18E-09	5.46E-07	1.65E-04*

*Hydraulic properties of CT2 footwall were solved using the Gringarten and Witherspoon solution for fractured aquifers with a single vertical plane fracture. The other wells were solved using the Hantush (leaky) method.

The best model to explain the responses of the pumping test in CT3 (hanging wall) is the leaky aquifer model from Hantush (1959) (Table 4; Figure S2). A radial-type flow regime is established resulting in an almost perfect leaky response in the pumping well itself and the two zones most connected to the CT3, namely the CT1 (fault) and CT2 (fault). The response at CT2 (footwall) during this test is best explained by the Gringarten–Witherspoon model (as above), which emphasizes that this observation well is influenced by a high-permeability connection zone. Similar to the CT1 aquifer pumping test, the hydraulic conductivity calculated from CT3 (hanging wall) during this test is characteristic of limestone/dolostone, but the hydraulic conductivity calculated from CT2 (footwall) is higher than expected for intact shale formations. The hydraulic conductivity values calculated from CT2 (fault) and CT1 (fault) are similar, with CT2 fault being slightly lower than CT1 (fault). The average specific storage value (5.52×10^{-5} m^{-1}) of the aquifer as determined from the results for CT1 (fault), CT2 (fault), and CT2 (footwall) is characteristic of confined aquifers, with higher values obtained for the CT2 (fault and footwall) compared to CT1 (fault). As noted above, the specific storage of the aquifer as determined from the CT3 (hanging wall) is not representative of the aquifer because the method simply uses the radius of the pumping well.

Even though multiple analytical models were used to interpret the aquifer pumping tests in CT1 (fault) and CT3 (hanging wall), the results are generally consistent between the tests and with the fault geometry and hydraulic connections observed during drilling and well completion. We acknowledge that the parameter estimations are approximate, but our choices of analytical models are

appropriate from a hydrogeological perspective. As such, we accept the uncertainty in our hydraulic parameter estimates, but from these preliminary tests, we can tentatively conclude that the Champlain Thrust is a semiconfined (leaky) aquifer with a strong presence of vertical fractures at the fault, possibly the normal faults exposed in outcrop. The hydraulic conductivity values determined from CT2 (footwall) and CT3 (hanging wall) are similar between the tests, even though the hydraulic conductivity value calculated from CT2 (footwall) is higher than expected for shale formations. The main difference between the tests is that the hydraulic conductivity values calculated from CT1 (fault) and CT2 (fault) determined from the CT3 (hanging wall) pumping test were lower than those determined from the CT1 (fault) pumping test. Additionally, the specific storage values differ for all wells between the tests, but are consistent with the values for confined aquifers. However, due to the strong leaky response from the CT3 (hanging wall) aquifer pumping test, we can infer that the hanging wall may be semiconfined.

The results from the aquifer pumping tests are preliminary and may be biased by a number of factors. Using multiple analytical models to solve for the hydraulic parameters is not standard practice. Each model has its own set of assumptions. The Gringarten–Witherspoon method is appropriate for analyzing pumping test data from a pumping well situated along a vertical fracture and data from observation wells situated at different distances from that fracture. But, if a well off the fracture is pumped, this method is no longer suitable; therefore, an alternative model, here Hantush, is more appropriate. Ideally, pumping test data should be analyzed using a single analytical method that best represents the field site, but in complex hydrogeological settings, we argue that multiple models are best used (or a numerical model could be used).

Another limitation is that the length of the two aquifer pumping tests differed, with the CT1 (fault) test being 3 h longer. Hydraulic parameters are better constrained with longer tests, so ideally the tests should have been performed for a longer period (24–48 h), but this was not possible due to technical reasons. Most notably, the results are limited by the small number of wells. Aquifer parameters are best characterized by multiple long-term tests in different locations and within different geologic formations. Therefore, to fully understand the hydrogeology of the Champlain Thrust fault at Lone Rock Point, more wells are needed, and longer aquifer pumping tests should be performed in *all* structural features (hanging wall, fault, and footwall). The presence of karst certainly affected the drilling and pumping tests, terminating drilling in CT1 at the fault and CT3 in the hanging wall. Future drilling plans in this area must proceed with caution and avoid the karst regions in order to successfully characterize the subsurface hydrogeology.

DISCUSSION: INTEGRATING SURFACE AND SUBSURFACE DATA

Table 5 summarizes the key surface and subsurface observations, and how these relate to observations from other data sources. Structural and hydrogeologic observations of the Champlain Thrust fault reveal a complex system, with features like karst and normal faults playing a significant role. Structural observations of the outcrop reveal that the fault structure thickness of Champlain Thrust fault varies on the scale of a few meters and splays out into multiple strands. The intersection between the thrust and normal faults may play a role in the evolution of karst, as the calcite-cemented older fault breccia is likely more soluble than the surrounding dolostone. No karst features were noted in the exposed outcrop, yet the well drilling revealed potentially karstic flow pathways in the hanging wall and fault. This may indicate that volumetrically minor karst pathways can escape detection in outcrop studies, but assert control over groundwater flow patterns. The presence of karst introduces an element of unpredictability at the Champlain Thrust fault, because karst conduits cannot be mapped from the surface or predicted from structural models. Therefore, the role of karst in groundwater flow at the Champlain Thrust fault is difficult to constrain, especially with the limited amount of karst data collected from the wells, leaving a number of questions unanswered. Is karst concentrated along younger faults that crosscut the Champlain Thrust fault (i.e., normal faults that intersect with the Champlain Thrust fault at the well-field site) or is

Table 5 Summary of key surface and subsurface observations.

Key surface observations	Related subsurface observation
1. Gently dipping, undulating fault geometry locally crosscut by minor normal faults	Depth to fault surface has tens of 10s m offset in short distance, consistent with offset by normal fault
2. Minor changes in fault core thickness	Difficult to determine the variation in fault thickness because only one well drilled through fault
3. Seep distribution indicates groundwater flow paths and the water table in fault or footwall	Large, hanging wall fractures (and karst?) drain the hanging wall near the cliff face locally lowering the water table
Key subsurface observations	**Related surface observation**
1. Significant vertical offset of the fault between wells	Consistent with exposed normal faults with unknown throw
2. Dominant, karstic flow pathways in the hanging wall and fault	Karst features not obvious in exposed hanging wall nor exposed fault core, but seen elsewhere in Dunham Formation
3. Water table near surface	Seeps primarily present in footwall

it prevalent throughout the subsurface, or is it concentrated along the ancient thrust surface? Does karst play a role in lowering the water table elevation at the outcrop?

The structural observations of the outcrop assisted in the interpretation of the distribution of groundwater seeps. Seeps were common in the footwall, with a few occurring at fault intersections, such as the normal fault, fault core, or where the fault splays out into multiple strands. The footwall is more fractured compared with the hanging wall, so it is likely that unsealed fractures would provide more pathways for groundwater flow and therefore more seepage. The occurrence of seeps at fault intersections indicates that these faults may be acting as conduits. Groundwater seeps provide a minimum water table elevation, suggesting the water table at the outcrop is at the elevation of the fault and flow in the hanging wall is limited. These observations may be biased, however, due to the inaccessibility of the hanging wall for a large portion of the outcrop. Large hanging wall fractures (and possibly karst) would have to drain the hanging wall near the cliff face to locally lower the water table, but fractures such as these, or karst, were not observed in outcrop. Future investigation should aim to make detailed seep observations at multiple times throughout the year, in order to gain a greater understanding of the seep distribution and water table elevation at the outcrop.

The aquifer pumping tests in CT1 and CT3 reveal a complex hydrogeologic system with karst and steep fractures (normal fault) as strong hydraulic conduits. Tentatively, the Champlain Thrust fault is a semiconfined (leaky) aquifer, with a presence of vertical fractures at the fault due to a younger fault or set of faults crosscutting the main fault. However, the results from the aquifer pumping tests are preliminary and limited by the lack of long-term pumping test data in all structural features (footwall, fault, and hanging wall).

The purpose of examining groundwater seeps and performing aquifer pumping tests is to gain a better understanding of the hydraulic properties of the aquifer. The groundwater seeps provide an estimate of the groundwater flux out of the outcrop itself, as well as an approximate water table elevation. The groundwater flux of the aquifer at the well-field site to the outcrop can be determined using Darcy's Law:

$$q = -KA\frac{dh}{dl}$$

where q is the groundwater flux (m sec^{-1}); K is the hydraulic conductivity (m sec^{-1}); A is the area of the outcrop; dh is the change in hydraulic head from the wells to the seeps (m); and dl is the distance from the wells to the outcrop (m). An effective hydraulic conductivity was calculated for the well-field site, knowing the hydraulic conductivity (determined from the pumping tests) and thickness of each unit. An estimate of groundwater flux was then derived from the effective hydraulic conductivity, the hydraulic gradient between the well-field site and outcrop, and the area of the outcrop below the water table. The groundwater flux from the well-field site to the outcrop is thus approximately 3.76×10^{-2} m^3 sec^{-1}, whereas the groundwater flux of the outcrop determined from frozen seep observations is 1.75×10^{-5} m^3 sec^{-1}. The fluxes differ by several orders of magnitude, suggesting that the seep fluxes are not representative of the full permeability of the area. This is likely due to the lower water table elevation in outcrop and/or groundwater flowing elsewhere. It must be noted that the flux values are estimates; the groundwater fluxes from the frozen seeps were roughly estimated using an approximate volume and approximate freezing time, which may affect the accuracy of the flux estimates. Moreover, seeps are discrete features and therefore not equivalent to the porous media-calculated fluxes from the aquifer pumping tests. Refining these estimates in future studies may produce more accurate groundwater flux estimates and more consistency between the two calculations.

Despite the surface and subsurface methods revealing different features of the hydrogeology of the Champlain Thrust fault (Table 5), we have developed a preliminary conceptual model of the study area (Fig. 8). At the outcrop, the fault core thickens on the meter scale, splays out into multiple strands, and is offset by a normal fault. The abundance of groundwater seeps in the footwall suggests that at the cliff face, the water table lowers to the elevation of the fault, making groundwater flow in the hanging wall limited. At the well-field site, the main fault is offset by a fault or set of faults. This, combined with localized occurrence of karst, creates a complex hydrogeologic system. In sum, these methods reveal the complexity and heterogeneity of the hydrogeology of the Champlain Thrust fault. Further research, by both structural geologists and hydrogeologists, is needed to better constrain and understand this complex system.

CONCLUSION

The spectacular exposure of the Champlain Thrust fault at Lone Rock Point is a natural laboratory, where structural and hydrogeological field data can be integrated to understand carbonate thrust fault hydrogeology. In outcrop, the fault core thickness varies on the meter scale, splays out into multiple strands, and is crosscut by a normal fault. Groundwater seeps are more prevalent in the heavily fractured footwall and limited at fault intersections, such as the normal fault (station 1, Fig. 2), multistranded segments of the fault (station 2, Fig. 2), fault core, and the hanging wall. This suggests that at the cliff face, the water table is generally located at the elevation of the fault and that groundwater flow in the hanging wall is limited. However, these observations are preliminary and may be biased due to the inaccessibility of the hanging wall/fault core.

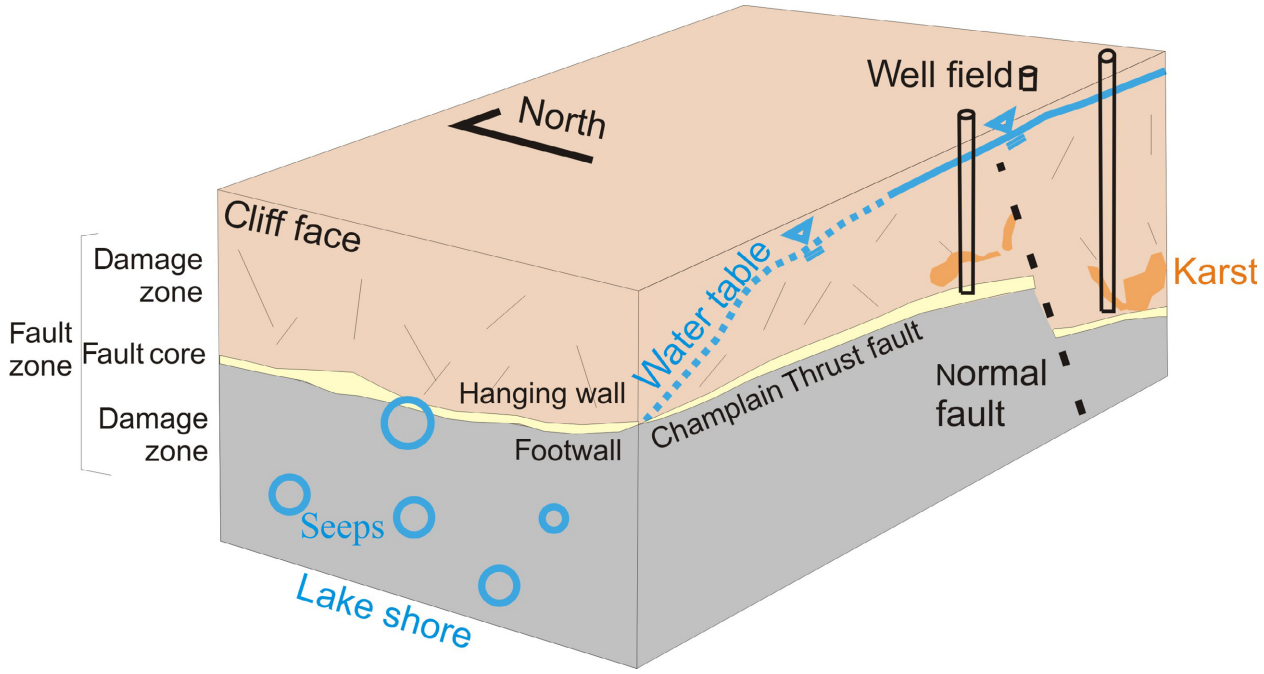

Fig. 8. Three-dimensional conceptual model of the Champlain Thrust fault.

Results from two aquifer pumping tests in the hanging wall and fault reveal a complex hydrogeological system. Multiple analytical models were used to estimate the aquifer parameters because the system did not meet any of the strict conceptual model criteria for any particular method. From this, it can tentatively be concluded that the aquifer may be semiconfined (leaky), with a strong presence of vertical fractures at the fault due to a fault or set of faults that crosscut the main fault at the well-field site. However, these results are preliminary and must be confirmed with long-term tests in multiple wells.

Two striking features were observed from drilling wells near the outcrop—the strong presence of karst and large disparity of fault depth. The normal fault identified along the outcrop, although crudely constrained, may be the cause of this significant offset. These features have a substantial effect on understanding the geology and hydrogeology of the area and should be further explored in the future.

The aim of this study was to establish an understanding of the hydrogeology of the Champlain Thrust fault using a multidisciplinary approach. The three approaches (structural geology observations, groundwater seep observations, and hydrogeological observations from wells) all revealed different aspects of the Champlain Thrust fault, but can be integrated into a preliminary conceptual model (Fig. 8). These methods expose the complexity and heterogeneity of the hydrogeology of the Champlain Thrust fault, an old, well-exposed fault in sedimentary rock.

ACKNOWLEDGEMENTS

The authors are grateful to the Episcopal Diocese of Vermont who provided access and logistical support for the project, especially from Chuck Courcey. The project also benefited from field help from Mikhail Smilovic and Mark Ranjram, discussions with J. Kim and K. Klepis and funding by the Canadian Foundation for Innovation and McGill University.

CONFLICT OF INTEREST

The authors declare no conflict of interest.

REFERENCES

Agosta F, Kirschner DL (2003) Fluid conduits in carbonate-hosted seismogenic normal faults of central Italy. *Journal of Geophysical Research*, **108**, 2221. doi: 10.1029/2002JB002013.

Agosta F, Mulch A, Camberline P, Aydin A (2008) Geochemical traces of CO_2 rich fluid flow along normal faults in central Italy. *Geophysical Journal International*, **174**, 758770.

Allen D, Michel FA (1999) Characterizing a faulted aquifer by field testing and numerical simulation. *Ground Water*, **37**, 718–28.

Andrews J, Burgess W, Edmunds W, Kay R, Lee D (1982) The thermal springs of Bath. *Nature*, **298**, 339–43.

Aydin A (2000) Fractures, faults, and hydrocarbon entrapment, migration and flow. *Marine and Petroleum Geology*, **17**, 797–814.

Ball LB, Ge S, Caine JS, Revil A, Jardani A (2010) Constraining fault-zone hydrogeology through integrated hydrological and geoelectrical analysis. *Hydrogeology Journal*, **18**, 1057–67.

Bense VF, Person M (2006) Faults as conduit–barrier systems to fluid flow in siliciclastic sedimentary aquifers. *Water Resources Research*, **42**, W05421. doi: 10.1029/2005WR004480.

Bense V, Person M, Chaudhary K, You Y, Cremer N, Simon S (2008) Thermal anomalies as indicator of preferential flow along faults in an unconsolidated sedimentary aquifer system. *Geophysical Research Letters*, **35**, L24406. doi: 10.1029/2008GL036017.

Bense VF, Gleeson T, Loveless SE, Bour O, Scibek J (2013) Fault zone hydrogeology. *Earth Science Reviews*, **127**, 171–192.

Berkowitz B (2002) Characterizing flow and transport in fractured geological media: a review. *Advances in Water Resources*, **25**, 861–84.

Billi A, Valle A, Brilli M, Faccenna C, Funiciello R (2007) Fracture-controlled fluid circulation and dissolutional weathering in sinkhole-prone carbonate rocks from central Italy. *Journal of Structural Geology*, **29**, 385–95.

Bredehoeft JD (1997) Fault permeability near Yucca Mountain. *Water Resources Research*, **33**, 2459–63.

Breesch L, Swennen R, Vincent B (2009) Fluid flow reconstruction in hanging and footwall carbonates: compartmentalization by Cenozoic reverse faulting in the Northern Oman Mountains (UAE). *Marine and Petroleum Geology*, **26**, 113–28.

Burbey T (2008) The influence of geologic structures on deformation due to ground water withdrawal. *Ground Water*, **46**, 202–11.

Caine JS, Evans JP, Forster CB (1996) Fault zone architecture and permeability structure. *Geology*, **24**, 1025–8.

Celico F, Petrella E, Celico P (2006) Hydrogeological behaviour of some fault zones in a carbonate aquifer of Southern Italy: an experimentally based model. *Terra Nova*, **18**, 308313.

Chambefort I, Buscarlet E, Wallis IC, Sewell S, Wilmarth M (2016) Ngatamariki Geothermal Field, New Zealand: geology, geophysics, chemistry and conceptual model. *Geothermics*, **59**, Part B: 266–80. ISSN 0375-6505, http://dx.doi.org/10.1016/j.geothermics.2015.07.011.

Davatzes N, Hickman SH (2010) Stress, fracture, and fluid-flow analysis using acoustic and electrical image logs in hot fractured granites of the Coso Geothermal Field, California, U.S.A. In: *Dipmeter and Borehole Image Log Technology*, vol. 92 (eds Pöppelreiter M, García-Carballido C, Kraaijveld M, AAPG Memoir), pp. 259–93. American Association of Petroleum Geologists,Danvers, MA. doi: 10.1306/13181288M923134.

Deitchman RS, Loheide SP II (2009) Ground-based thermal imaging of groundwater flow processes at the seepage face. *Geophysical Research Letters*, **36**, L14401.

Doan ML, Cornet FH (2007) Thermal anomaly near the Aigio fault, Gulf of Corinth, Greece, maybe due to convection below the fault. *Geophysical Research Letters*, **34**, L0631.

Dockrill B, Shipton Z (2010) Structural controls on leakage from a natural CO2 geologic storage site: central Utah, U.S.A. *Journal of Structural Geology*, **32**, 1768–1782, (2012).

Douglas M, Clark I, Raven K, Bottomley D (2000) Groundwater mixing dynamics at a Canadian Shield mine. *Journal of Hydrology*, **235**, 88–103.

Duffield GM (2007) *AQTESOLV for Windows Version 4.5 User's Guide*. HydroSOLVE Inc., Reston, VA.

Evans JP, Forster CB, Goddard JV (1997) Permeability of fault-related rocks, and implications for hydraulic structure of fault zones. *Journal of Structural Geology*, **19**, 1393–404.

Faulkner D, Jackson C, Lunn R, Schlische R, Shipton Z, Wibberley C, Withjack M (2010) A review of recent developments concerning the structure, mechanics and fluid flow properties of fault zones. *Journal of Structural Geology*, **32**, 1557–75.

Freeze RA, Cherry JA (1979) *Groundwater*. Prentice Hall Inc., Upper Saddle River, New Jersey.

Gringarten AC, Witherspoon PA (1972) A method of analyzing pump test data from fractured aquifers. Proc. Symp. Percolation through Fissured Rock, Sept. 18–19, 1971, Stuttgart, pp. T3-B-1 to T3-B-8. International Society for Rock Mechanics and International Association of Engineering Geology.

Hantush MS (1959) Nonsteady flow to flowing wells in leaky aquifers. *Journal of Geophysical Research*, **64**, 2156–202.

Hayman NW, Kidd WSF (2002) Reactivation of prethrusting, synconvergence normal faults as ramps within the Ordovician Champlain-Taconic thrust system. *Geological Society of America Bulletin*, **114**, 476–89.

Kampman N, Burnside NM, Shipton ZK, Chapman HJ, Nicholl JA, Ellam RM, Bickle MJ (2012) Pulses of carbon dioxide emissions from intracrustal faults following climatic warming. *Nature Geoscience*, **5**, 352–8.

Kim J, Ryan P, Klepeis K, Gleeson T, North K, Bean J, Davis L, Filoon J (2014) Tectonic evolution of a Paleozoic thrust fault influences the hydrogeology of a fractured rock aquifer, northeastern Appalachian foreland. *Geofluids*, **14**, 266–90.

Lopez D, Smith L (1996) Fluid flow in fault zones: influence of hydraulic anisotropy and heterogeneity on the fluid flow and heat transfer regime. *Water Resources Research*, **32**, 3227–35.

Mal'kovskii V, Pek A (2001) Evaluation of the influence of a highly permeable fault on transport of pollutants by the local groundwater flow. *Geology of Ore Deposits*, **43**, 216–23.

Mayer A, May W, Lukkarila C, Diehl J (2007) Estimation of fault-zone conductance by calibration of a regional groundwater flow model: desert Hot Springs, California. *Hydrogeology Journal*, **15**, 10931106.

McNamara DD, Massiot C, Lewis B, Wallis IC (2015) Heterogeneity of structure and stress in the Rotokawa Geothermal Field, New Zealand. *Journal of Geophysical Research: Solid Earth*, **120**, 1243–1262.

McNamara DD, Sewell S, Buscarlet E, Wallis IC (2016) A review of the Rotokawa Geothermal Field, New Zealand. *Geothermics*, **59**, Part B: 281–93. ISSN 0375-6505, http://dx.doi.org/10.1016/j.geothermics.2015.07.007.

Micarelli L, Benedicto A, Wibberley CAJ (2006) Structural evolution and permeability of normal fault zones in highly porous carbonate rocks. *Journal of Structural Geology*, **28**, 1214–27.

Mroczek EK, Milicich SD, Bixley PF, Sepulveda F, Bertrand EA, Soengkono S, Rae AJ (2016) Ohaaki geothermal system: refinement of a conceptual reservoir model. *Geothermics*, **59**, Part B: 311–24. ISSN 0375-6505, http://dx.doi.org/10.1016/j.geothermics.2015.09.002.

Mundy E, Gleeson T, Roberts M, McKenzie JM. Thermal imagery of groundwater seeps: possibilities and limitations. *Groundwater*, doi: 10.1111/gwat.12451. [Epub ahead of print]

Ofoegbou GI, Painter S, Chen R, Randall WF, Ferril DA (2001) Geomechanical and thermal effects on moisture flow at the proposed Yucca mountain nuclear waste repository. *Nuclear Technology*, **134**, 241–62.

Ratcliffe NM, Stanley RS, Gale MH, Thompson PJ, Walsh GJ (2011) Bedrock geologic map of Vermont: U.S. Geological Survey Scientific Investigations Map3184, 3 sheets, scale 1:100 000.

Revil A, Cuttler S, Karaoulis M, Zhou J, Raynolds B, Batzle M (2015) The plumbing system of the Pagosa thermal Springs, Colorado: application of geologically constrained geophysical inversion and data fusion. *Journal of Volcanology and Geothermal Research*, **299**, 1–18, ISSN 0377-0273, http://dx.doi.org/10.1016/j.jvolgeores.2015.04.005.

Rowland JV, Sibson RH (2004) Structural controls on hydrothermal flow in a segmented rift system, Taupo Volcanic Zone, New Zealand. *Geofluids*, **4**, 259–83.

Rowley DB (1983) Contrasting fold-thrust relationships along northern and western edges of the Taconic allochthons; Implications for a two-stage emplacement history. *Geological Society of America Abstracts with Programs*, **15**, 174.

Rowley DB, Kidd WSF (1981) Stratigraphic relationships and detrital composition of the medial Ordovician flysch of western New England: implications for the tectonic evolution of the Taconic orogeny. *The Journal of Geology*, **89**, 199–218.

Savage HM, Brodsky EE (2010) Collateral damage: evolution with displacement of fracture distribution and secondary fault strands in fault damage zones. *Journal of Geophysical Research*, **116**, 14.

Scholz C, Anders C (1994) The permeability of faults. Proceedings of Workshop LXIII, The Mechanical Involvement of Fluids in Faulting, U.S. Geol. Surv. Open File Rep. 94-228, 247–253.

Shipton Z, Evans J, Kirchner D, Kolesar P, Williams A, Heath J (2004) Analysis of CO_2 leakage through low-permeability faults from natural reservoirs in the Colorado Plateau, southern Utah. In: *Geological Storage of Carbon Dioxide* (eds Baines S, Worden R), pp. 43–58. vol. 233 of Special Publications. Geological Society, London.

Smith L, Forster CB, Evans JP (1991) Interaction between fault zones, fluid flow and heat transfer at the basin scale. In: *Hydrogeology of Low Permeability Environments*, vol. 2 (eds Newman SP, Neretnieks I), pp. 41–67. International Association of Hydrological Sciences Selected Papers in Hydrogeology, Washington. D.C.

Sorkhabi R, Tsuji Y (2005) *Faults, Fluid Flow & Petroleum Traps.* vol. 85 of AAPG Memoir. American Association of Petroleum Geologists, Tulsa.

Spane FA Jr, Wurstner SK (1993) DERIV: A Program for Calculating Pressure Derivatives for Use in Hydraulic Test Analysis. *GroundWater*, **31**, 814–822.

Stanley R (1987) The Champlain thrust fault, lone rock point, Burlington, Vermont. *Geological Society of America Centennial Field Guide—Northeastern Section*, **7**, 63–6.

Stanley RS, Ratcliffe NM (1983) Simplified lithotectonic synthesis of the pre-Silurian eugeoclinal rocks of western New England: Vermont Geological Survey Special Bulletin No. 5.

Stanley RS, Ratcliffe NM (1985) Tectonic synthesis of the Taconic orogeny in western New England. *Geological Society of America Bulletin*, **96**, 1227–50.

Stanley RS, Sarkesian A (1972) Analysis and chronology of structures along the Champlain thrust west of the Hinesburg synclinorium. In: *Guidebook for Field Trips in Vermont, 64th Annual Meeting of the New England Intercollegiate Geological Conference, Burlington, Vermont*. pp. 117–49.

Tueckmantel C, Fisher QJ, Manzocchi T, Skachkov S, Grattoni CA (2012) Two-phase fluid flow properties of cataclastic fault rocks: implications for CO2 storage in saline aquifers. *Geology*, **40**, 39–42.

Wibberly CAJ (2002) Hydraulic diffusivity of fault gouge zones and implications for thermal pressurization during seismic slip. *Earth, Planets and Space*, **54**, 1153–71.

SUPPORTING INFORMATION

Additional Supporting Information may be found online in the supporting information tab for this article:

Figure S1. (A) Drawdown and (B) derivative of CT1 (fault) during the 12-hour aquifer-pumping test.

Figure S2. (A) Drawdown and (B) derivative of CT3 (hanging wall) during the 9-hour aquifer-pumping test.

GEOFLUIDS

Volume 16, Number 4, November 2016
ISSN 1468-8115

CONTENTS

WILEY Blackwell

Geofluids* is abstracted/indexed in *Chemical Abstracts

This journal is available online at Wiley Online Library. Visit onlinelibrary.wiley.com to search the articles and register for table of contents and e-mail alerts.